

A new sulcal landmark identifying anatomical and functional gradients in human lateral prefrontal cortex

Jacob A. Miller^{1*}, Willa I. Voorhies^{1,2}, Daniel J. Lurie², Mark D'Esposito^{1,2}, Kevin S. Weiner^{1,2}

¹Helen Wills Neuroscience Institute, ²Department of Psychology,
University of California-Berkeley

***Corresponding author:**

Jacob A. Miller
jacob_miller@berkeley.edu
210 Barker Hall
University of California-Berkeley
Berkeley, CA, 94720

Keywords: prefrontal cortex, functional neuroanatomy, morphology, gradients, connectivity, brain mapping

Abstract

Understanding the relationship between anatomy and function in portions of human cortex that are expanded compared to other mammals such as lateral prefrontal cortex (LPFC) is of major interest in cognitive neuroscience. Implementing a multi-modal approach and the manual definition of nearly 800 cortical indentations, or sulci, in 72 hemispheres, we report a new sulcal landmark in human LPFC: the *posterior middle frontal sulcus (pmfs)*. The *pmfs* is a shallow tertiary sulcus with three components that differ in their myelin content, resting state connectivity profiles, and engagement across meta-analyses of 83 cognitive tasks. These findings support a classic, largely unconsidered anatomical theory that tertiary sulci serve as landmarks in association cortices, as well as a modern cognitive neuroscience theory proposing a functional hierarchy in LPFC. As there is a growing need for computational tools that automatically define tertiary sulci throughout cortex, we share *pmfs* probabilistic sulcal maps with the field.

Introduction

Understanding how anatomical structures of the brain support functional gradients and networks that perform computations for human-specific aspects of cognition is a major goal in systems and cognitive neuroscience. Of the many anatomical structures to target, lateral prefrontal cortex (LPFC), which is disproportionately expanded in the human brain, is particularly important given its central role in cognitive control and goal-directed behavior¹⁻⁴. Major progress has been made in understanding the relationship between the functional organization and the large-scale cortical anatomy of human LPFC. For example, modern neuroimaging research shows widespread support for a hierarchical functional gradient organized along the rostral-caudal anatomical dimension of LPFC spanning several centimeters⁵⁻⁷. Beyond this large-scale organization of human LPFC, it is unknown if more fine-grained structural-functional relationships exist. Thus, to begin to fill this gap in knowledge, we sought to answer the following question in the present study: Do individual differences in finer-scale morphological features of cortical anatomy predict anatomical and functional gradients in human LPFC?

An important morphological feature of cortex is the patterning of the indentations, or sulci. Indeed, 60-70% of the cortex is buried in sulci and some sulci serve as landmarks that identify different cortical areas, especially in primary sensory cortices⁸⁻¹¹. In these cases, merely identifying a sulcus provides functional insight⁸⁻¹¹. Despite this widely replicated relationship between sulcal morphology and functional representations in primary sensory cortices, much less is known regarding the predictability between sulcal landmarks and functional representations in association cortex, especially LPFC. A classic theory proposed by Sanides (1964) hypothesized that shallow, tertiary sulci, which emerge last in gestation and continue to develop after birth, would serve as landmarks in association cortices¹². The logic behind this hypothesis is that the protracted development of tertiary sulci may result from their demarcation of architectural gradations in cortex that are in turn, functionally and behaviorally relevant. Moreover, their

Miller et al. | A new sulcal landmark in human prefrontal cortex

protracted development may co-occur with, or enable, cognitive functions that also show a protracted development, such as working memory, or inhibitory control, each of which have been linked to the LPFC^{6,13-17}.

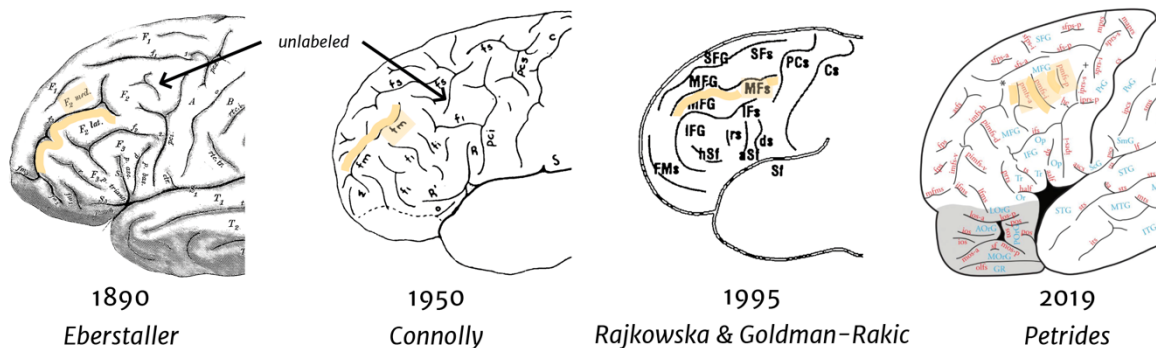
However, at least two factors have prevented the examination of tertiary sulci relative to anatomical and functional gradients in human LPFC. First, tertiary sulci are presently excluded from nearly all published neuroanatomical atlases because classic anatomists could not discriminate tertiary sulci from indentations produced by veins and arteries on the outer surface of the cerebrum in post-mortem tissue, which is considered the gold standard of anatomical research¹⁸. Consequently, the patterning of tertiary sulci within LPFC has a contentious history, whereby sulci in the posterior middle frontal gyrus (MFG) were either undefined in classic atlases or conflated with more anterior structures (**Fig. 1**). Second, the majority of human functional neuroimaging studies implement group analyses on average brain templates. As shown in **Fig. 1**, averaging cortical surfaces together causes tertiary sulci in LPFC to disappear, especially within the posterior MFG. Thus, while recent studies have identified meaningful individual differences in functional brain organization in LPFC^{19,20}, these differences have not been linked or attributed to i) individual differences in sulcal anatomy or ii) microanatomical properties.

Here, we implemented a multi-modal approach demonstrating that carefully identifying individual sulci in LPFC reveals that the *posterior middle frontal sulcus (pmfs)* is a new sulcal landmark for functional and anatomical gradients in human LPFC. We applied a recently proposed labeling scheme of tertiary sulci in LPFC^{21,22} from post-mortem brains to test whether these sulci could be defined in the LPFC of individual subjects *in-vivo*. We find that three components of the *pmfs* are dissociable based on myelin content, resting state functional connectivity profiles, and cognitive task activations. Together, these results not only provide important evidence that individual differences in LPFC sulcal patterning reflects meaningful differences in the cortical

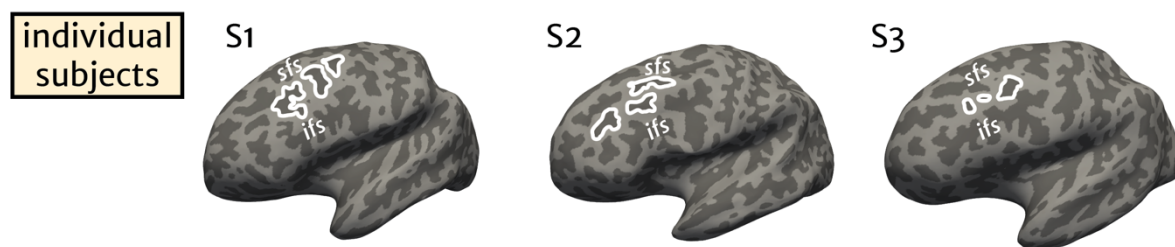
Miller et al. | A new sulcal landmark in human prefrontal cortex

layout of anatomical and functional gradients, but also provides empirical support for Sanides' classic hypothesis.

a historical ambiguity regarding the middle frontal sulci (pmfs)



b identification of the middle frontal sulci (pmfs) within individuals



c prefrontal landmarks are absent from template and average brains

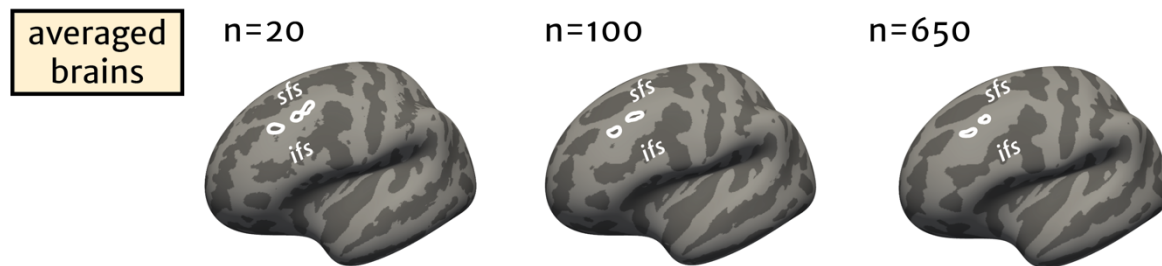


Figure 1. A synopsis of ambiguity regarding sulcal definitions in the human posterior middle frontal gyrus over the last 130 years. Classic and modern schematics of the sulcal patterning in human lateral prefrontal cortex (LPFC). (a) Sulci in the middle frontal gyrus are labeled in yellow on classic and modern schematics of human LPFC. Historically, anatomists had previously either (a) not labeled the sulci within the location of the modern pmfs (first two images; arrow indicates depicted, but unlabeled sulcal components)^{23,24} or b) included these sulci in the definition of the posterior portion of the frontomarginal sulcus (third image)²⁵. The most recent schematic^{21,22} proposes that the pmfs is separate from the intermediate frontal sulcus (*imfs-h* and *imfs-v*, synonymous with the *frontomarginal sulcus*) and consists of three distinct components: posterior (*pmfs-p*), intermediate (*pmfs-i*), and anterior (*pmfs-a*). (b) Three individually labeled left hemispheres with the pmfs outlined in white. The pmfs is prominent within individual subjects (**Supplemental Fig. 1** for all subjects). The superior and inferior frontal sulci (*sfs*, *ifs*) are labeled for reference above and below the middle frontal gyrus, respectively. (c) Average cortical surfaces show much smaller pmfs components compared to individual subjects. As more subjects are averaged together into templates, the pmfs disappears almost entirely, which is inconsistent with their prominence in individual hemispheres.

Results

Historic and modern definitions of sulci within the middle frontal gyrus (MFG) are contradictory. For example, sulcal definitions within the MFG vary in a) their nomenclature, b) the number of sulcal components depicted or acknowledged in schematics, c) the omission or inclusion of sulci within the posterior MFG, and d) the actual empirical data that is included to support the illustration of the sulcal patterning (**Fig. 1**). To ameliorate these concerns and to either empirically support or to refute the generality of sulcal definitions within the posterior MFG, we apply a classic, multimodal approach that has been used to distinguish cortical areas from one another in order to determine sulcal definitions in the posterior MFG. Specifically, after identifying each sulcus within the posterior MFG based on a recent proposal in post-mortem human brains^{22,26}, we use both anatomical and functional MRI data to either support or refute the identification of individual sulci within this cortical expanse. Implementing this two-pronged approach, we first examined if the three components of the posterior middle frontal sulcus (*pmfs*) are consistently identifiable within individual hemispheres. And if so, we then tested if the three *pmfs* components are anatomically and functionally homogenous, or serve as landmarks identifying anatomical and functional heterogeneity in LPFC. This approach supports the latter in which there are three anatomically and functionally distinct sulci within the posterior MFG: the posterior (*pmfs-p*), intermediate (*pmfs-i*), and anterior (*pmfs-a*) posterior middle frontal sulci.

Three posterior middle frontal sulci (pmfs) are identifiable within individual subjects and are characteristically shallow

Before examining the sulcal patterning within the posterior MFG, we first identified reliable sulci (**Methods: manual sulcal labeling**) surrounding the MFG in both *in vivo* cortical surface reconstructions and post-mortem brains (**Fig 2a**). Posteriorly, we identified the central sulcus (cs), as well as the superior (*sprs*) and inferior (*iprs*) pre-central sulci. Superiorly, we identified the

Miller et al. | A new sulcal landmark in human prefrontal cortex

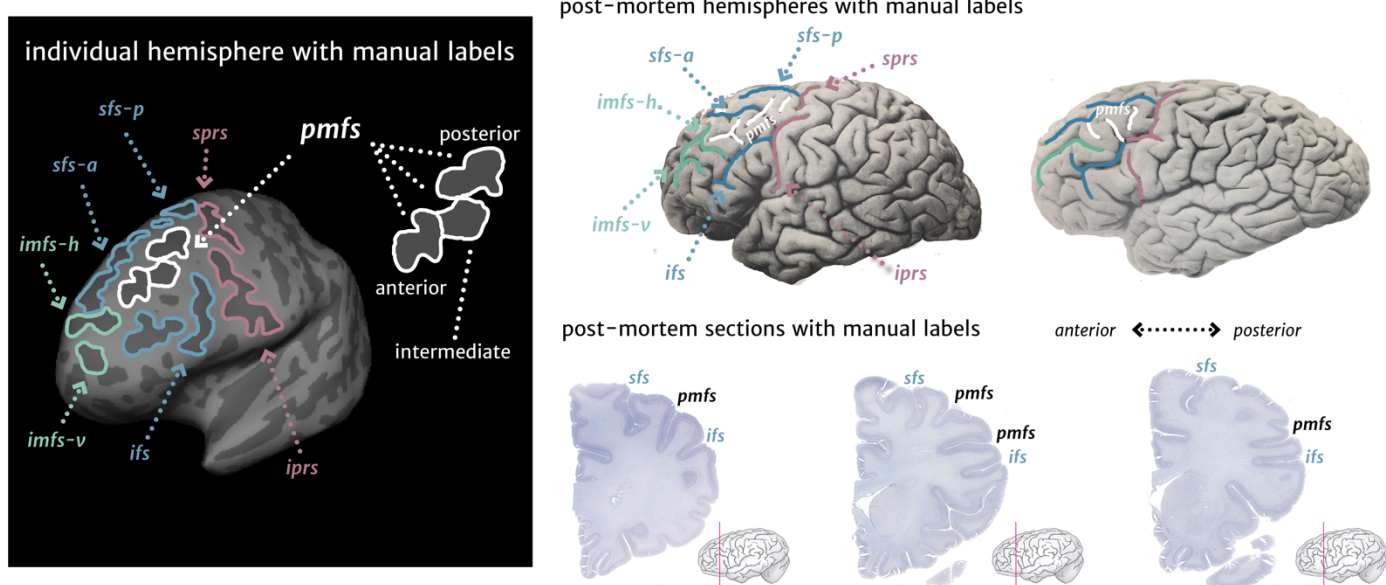
anterior (*sfs-a*) and posterior (*sfs-p*) superior frontal sulci. Inferiorly, we identified the inferior frontal sulcus (*ifs*). Anteriorly, we identified the horizontal (*imfs-h*) and vertical (*imfs-v*) intermediate frontal sulci. The latter two sulci are consistent with Eberstaller's classic definition of the middle frontal sulcus, but have since been renamed (**Fig 1**)^{21,22}. Within the posterior MFG, we identified three sulci in every hemisphere (N=72). From posterior to anterior, the first sulcus (*pmfs-p*) is positioned immediately anterior to the *sprs* (**Fig. 2a, Supplemental Fig. 1**), and most commonly does not intersect other sulci (**Supplemental Table 1** for a summary of the morphological patterns, or types). The second sulcus (*pmfs-i*) is located immediately anterior to the *pmfs-p*, and typically aligns with the separation between the *sfs-a* and *sfs-p* components. The *pmfs-i* is most often independent (especially in the right hemisphere) or intersects (especially in the left hemisphere) the *pmfs-a*. Finally, the third sulcus (*pmfs-a*) is immediately anterior to the *pmfs-i*, inferior to the *sfs-a*, and posterior to the *imfs-h*. The *pmfs-a* most commonly intersects other sulci in the right hemisphere. Each sulcus is also identifiable within individual *in-vivo* volumetric slices (**Supplemental Fig. 2**) and in postmortem brains (**Fig. 2; Supplemental Fig. 3**), which indicates that the computational process used to generate the cortical surface reconstruction in the MRI data does not artificially create these sulci within the middle frontal gyrus.

The two most identifying morphological features of the three *pmfs* sulci are their surface area (**Fig. 2a**) and depth (**Fig. 2b**). Each *pmfs* sulcus is of roughly equal surface area (**Fig. 2b, Supplemental Table 2**), which is smaller than the surface area of the other examined sulci in LPFC (**Fig. 2b, Supplemental Table 3**). A two-way repeated-measures ANOVA with factors sulcus and hemisphere yielded a main effect of sulcus ($F(5.78, 202.15) = 384.1, p < 0.001, \eta^2_G = 0.84$) and no main effect of hemisphere ($F(1, 35) = 0.1, p = 0.77$). The three *pmfs* sulci are also the shallowest of the lateral PFC sulci examined (**Fig. 2c, Supplemental Table 2**). A two-way ANOVA with sulcus and hemisphere as factors yielded a main effect of sulcus ($F(3.15, 103.84) = 77.7, p < 0.001, \eta^2_G$

Miller et al. | A new sulcal landmark in human prefrontal cortex

= 0.55), and a main effect of hemisphere ($F(1, 33) = 20.4, p < 0.001, \eta^2_G = 0.02$) in which sulci were deeper in the right compared to the left hemisphere (**Fig. 2b, Supplemental Table 3**). Post-hoc tests show that, across hemispheres, the *pmfs-p* is shallower than all other sulci (p -values < 0.001 , Tukey's adjustment), while the *pmfs-i* and *pmfs-a* are shallower than all other sulci except for the *imfs-v*. Taken together, three *pmfs* sulci are identifiable in individual hemispheres (**Fig. 2, Supplemental Fig 1**) and distinguish themselves from other LPFC sulci based on their surface area and shallowness.

a sulcal labels



b sulcal morphology

lateral frontal sulci

central	cs
inferior precentral	iprs
superior precentral	sprs
inferior frontal	ifs
posterior middle frontal, posterior	pmfs-p
posterior middle frontal, intermediate	pmfs-i
posterior middle frontal, anterior	pmfs-a
superior frontal, posterior	sfs-p
superior frontal, anterior	sfs-a
intermediate frontal, horizontal	imfs-h
intermediate frontal, vertical	imfs-v

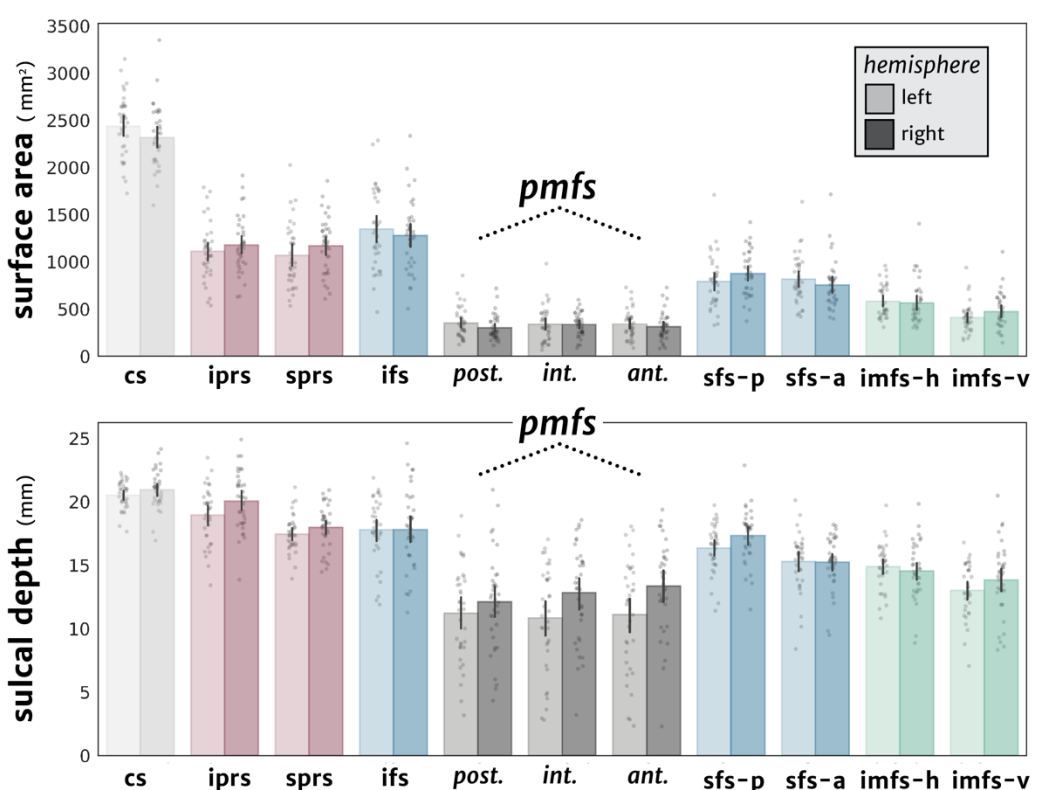


Figure 2. The pmfs sulci are easily identifiable and characteristically shallow. (a) Left, an example inflated cortical surface of an individual left hemisphere in which the sulci examined in the present study are outlined and labeled. Sulci are dark gray, while gyri are light gray. Right, two different post-mortem brains²⁷ and three histological sections (referred to as “intermediate frontal sulcus” in the Allen Human Brain Atlas: <https://atlas.brain-map.org/>)²⁸ showing that the pmfs sulci are also identifiable in post-mortem tissue samples. (b) Top: Surface area for each sulcus (ordered posterior to anterior) is plotted for each individual

Miller et al. | A new sulcal landmark in human prefrontal cortex

subject (gray circles), as well as the mean (colored bars) and 95% confidence interval (black line). Acronyms used for each LPFC sulcus are also included^{21,22}. Darker shades indicate right hemisphere values, while lighter shades indicate left hemisphere values. The three *pmfs* sulci have the smallest surface area of all sulci in LPFC. Bottom: Same layout as above, but for sulcal depth (mm), as calculated from a recent algorithm²⁹. The three *pmfs* sulci are the shallowest of all sulci in LPFC.

The pmfs-p, pmfs-i, and pmfs-a are anatomically dissociable and reflect a larger rostro-caudal myelination gradient in LPFC

While the *pmfs-p*, *pmfs-i*, and *pmfs-a* are morphologically distinct from surrounding sulci (**Fig. 2**), it is presently unknown if they are anatomically and functionally similar or distinct from one another. To test this, we first extracted and compared average MRI T_{1w}/T_{2w} ratio values from each sulcus. The T_{1w}/T_{2w} ratio is a tissue contrast enhancement index that is correlated with myelin content (**Fig. 3a**)^{30,31}. We chose this index because myeloarchitecture is a classic criterion used to separate cortical areas from one another^{12,31-35}. A two-way ANOVA with sulcus and hemisphere as factors yielded a main effect of sulcus ($F(1.76, 61.7) = 85.0, p < 0.001, \eta^2_G = 0.39$) and a main effect of hemisphere ($F(1, 35) = 10.5, p = 0.003, \eta^2_G = 0.05$) on myelin content, but no sulcus x hemisphere interaction, ($F(1.73, 60.5) = 2.5, p = 0.10$). The differences in myelin across sulci were driven by the finding that T_{1w}/T_{2w} decreased from posterior to anterior across hemispheres: *pmfs-p* vs. *pmfs-i*, $t(70) = 9.75, p < 0.001$ (Tukey's post-hoc), *pmfs-i* vs. *pmfs-a*, $t(70) = 2.62, p = 0.029$, *pmfs-p* vs. *pmfs-a*, $t(70) = 12.37, p < 0.001$. The right hemisphere also had higher myelin content overall in the *pmfs*, $t(35) = 3.25, p = 0.003$. Accordingly, the three sulci are differentiable based on myelin content in both hemispheres (**Fig. 3b**).

The rostro-caudal gradient among the *pmfs-p*, *pmfs-i*, and *pmfs-a* sulci is embedded within a larger rostro-caudal myelination gradient in lateral PFC. Specifically, modeling T_{1w}/T_{2w} content across frontal sulci as a function of distance from the central sulcus (**Fig. 3c**) using a mixed linear model revealed a significant, negative effect of distance from the central sulcus along the rostral-caudal axis ($\beta = -0.001, z = -33.8, p < 0.001$), with no differences between hemispheres ($\beta = -0.003, z = -$

Miller et al. | A new sulcal landmark in human prefrontal cortex

0.8, $p = 0.4$). Together, the *pmfs-p*, *pmfs-i*, and *pmfs-a* serve as sulcal landmarks that capture larger anatomical and functional hierarchical gradients in LPFC (see **Discussion** for further details).

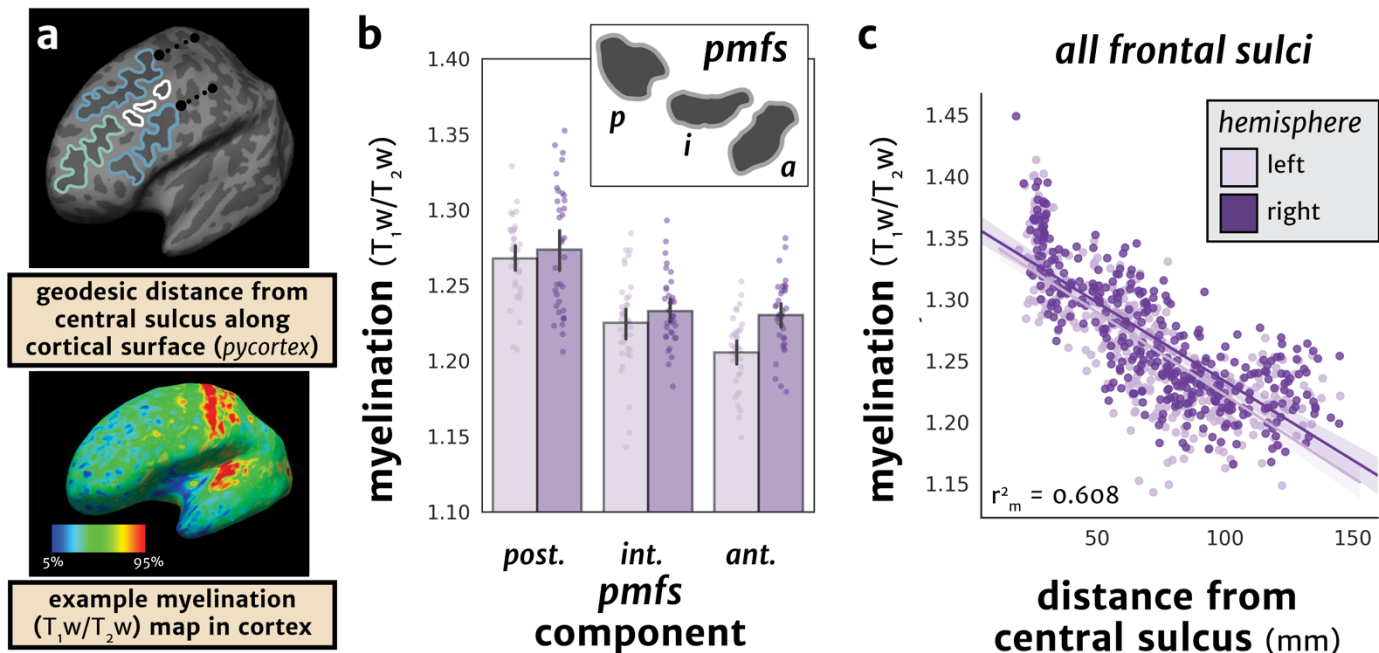


Figure 3. The pmfs sulci are anatomically differentiable based on myelin content. (a) Top: Schematic of the calculation of geodesic distance along the cortical surface. For each sulcus, the average distance of each vertex from the central sulcus was calculated (dotted black line; **Methods**). Bottom: an example T_1w/T_{12w} map in an individual subject in which 5-95% percentile of values are depicted. Tissue contrast enhancement (a proxy for myelin) is highest (warm colors) in primary sensorimotor areas. (b) Myelination (T_1w/T_{12w}) values plotted for each component of the pmfs for each individual subject ($n = 36$). Bars represent mean \pm 95% CI, while each subject is depicted as a circle. Darker shades indicate right hemisphere values, while lighter shades indicate left hemisphere values. The components of the pmfs are differentiable based on myelination content, with a decrease from posterior to anterior across both hemispheres. (c) Scatterplot showing the negative relationship between distance from the central sulcus to the mean myelination value for all labeled sulci from each individual ($N = 36$ subjects). The mixed linear model (**Methods**) with predictors of distance and hemisphere shows a marginal r^2 of 60.8%. Scatterplot is bootstrapped at 68% CI for visualization. *Dark purple*: right hemisphere; *Light purple*: left hemisphere.

The pmfs-p, pmfs-i, and pmfs-a exhibit different characteristic patterns of whole brain functional connectivity

To determine if the *pmfs-p*, *pmfs-i*, and *pmfs-a* are functionally distinct, we leveraged detailed individual functional parcellations of the entire cerebral cortex based on functional connectivity from a recently published study²⁰ (**Fig. 4a**). Importantly, this parcellation was conducted blind to both cortical folding and our sulcal definitions. Within each hemisphere in the same subjects in which we generated manual sulcal labels, we generated a functional connectivity network profile (which we refer to as a “connectivity fingerprint”). For each sulcal component we calculated the overlap (on the native hemisphere, based on the dice coefficient; **Methods**) between each sulcal label and 17 functional networks within the area of the sulcal component.

Our approach demonstrated that the *pmfs-p*, *pmfs-i*, and *pmfs-a* have different connectivity fingerprints and thus, are functionally dissociable. Average connectivity fingerprints across subjects are illustrated in **Fig. 4b**. A repeated-measures ANOVA with sulcal component (*pmfs-p*, *pmfs-i*, *pmfs-a*), hemisphere (left, right), and network yielded a significant component x network interaction ($F(32, 1120) = 45.2, p < 0.001, \eta^2_G = 0.29$), as well as a component x network x hemisphere interaction ($F(32, 1120) = 5.26, p < 0.001, \eta^2_G = 0.040$) (**Fig. 4b**). In each hemisphere, there is a component x network interaction (left: $F(32, 1120) = 29.4, p < 0.001, \eta^2_G = 0.35$, right: $F(32, 1120) = 23.2, p < 0.001, \eta^2_G = 0.27$) in which the difference between hemispheres is driven by the *pmfs-p* connectivity fingerprint. Specifically, the *pmfs-p* overlaps most with the default mode network in the left hemisphere and the cognitive control network in the right hemisphere.

Additionally, there are also individual and hemispheric differences in the connectivity fingerprint of each *pmfs* component at the single subject level (**Fig. 4c; Supplemental Fig. 4**). To quantify variability, we built on work showing network connectivity variability across individuals^{20,36} by relating connectivity variability to individual anatomical landmarks in LPFC. We characterized

Miller *et al.* | A new sulcal landmark in human prefrontal cortex

connectivity fingerprint variability by measuring the pairwise Wasserstein distance between the connectivity fingerprint profiles for all unique subject pairs for each sulcal component (see **Methods**). This approach quantifies how variable the pattern of network overlap within each *pmfs* component is across individuals. In the right hemisphere, the *pmfs-p* showed the most variable network profile across all unique subject pairs (*pmfs-p* vs. *pmfs-i*, Wilcoxon-Signed rank test, $W = 7.2 \times 10^4$, $p < 0.001$, *pmfs-p* vs. *pmfs-a*, $W = 7.4 \times 10^4$, $p < 0.001$), while the *pmfs-i* was most variable in the left hemisphere (*pmfs-i* vs. *pmfs-a*, $W = 8.8 \times 10^4$, $p = 0.014$, *pmfs-i* vs. *pmfs-p*, $W = 8.0 \times 10^4$, $p < 0.001$). This variability analysis suggests that the right *pmfs-p* and left *pmfs-i* mark regions of LPFC with particularly high levels of individual differences in functional connectivity profiles, providing an anatomical substrate for network connectivity differences across individuals.

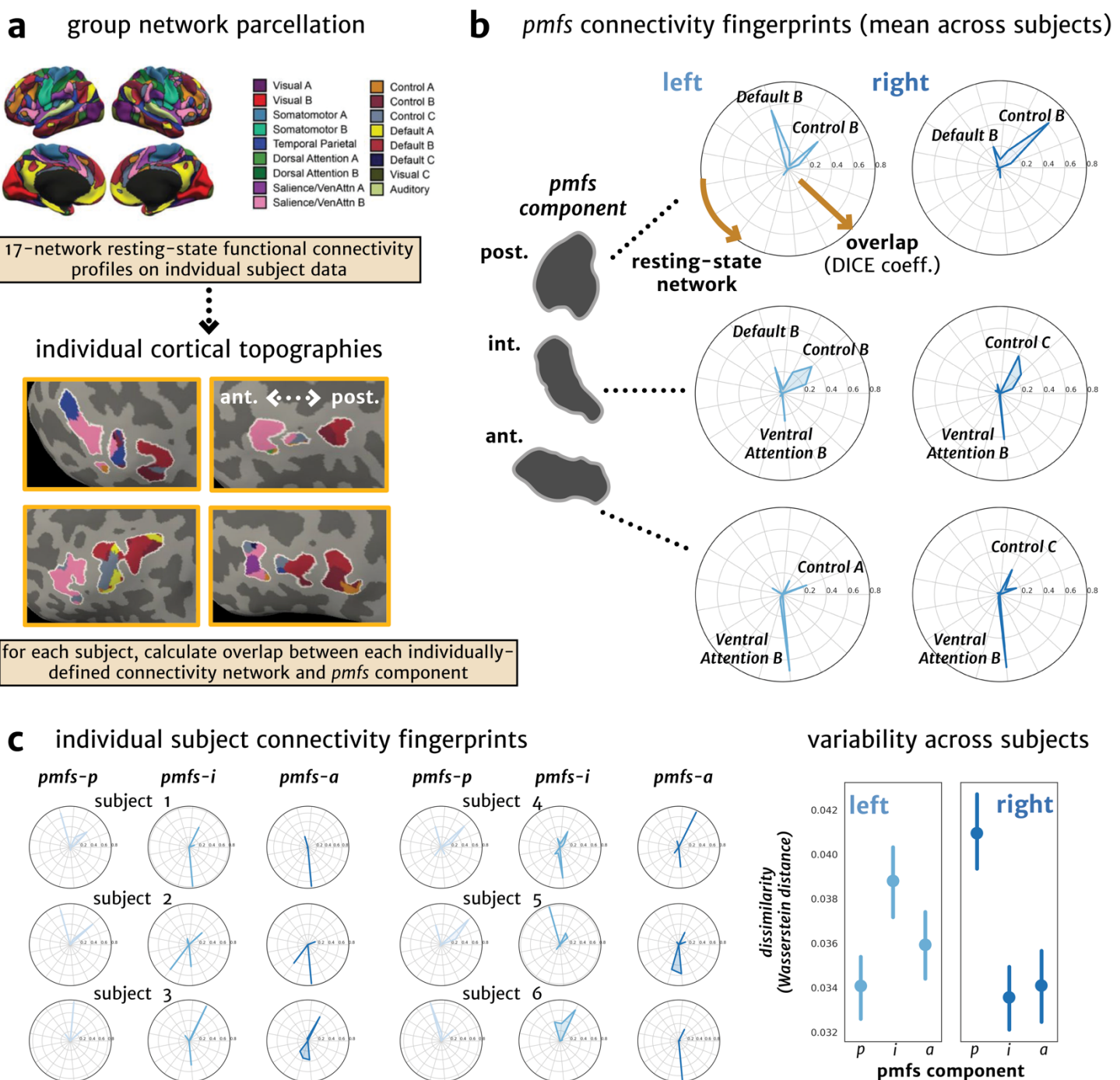


Figure 4. The pmfs components are functionally differentiable based on connectivity fingerprints within individual subjects. (a) Schematic of how individual-level resting state connectivity profiles were generated in each subject. Resting-state network parcellations for each subject were obtained from a recent study²⁰ in an observer-independent fashion of sulcal definitions in LPFC. Example individual connectivity profiles are shown in four individual subjects, colored according to the group parcellation. The individual connectivity profiles and pmfs sulcal definitions were used to calculate the connectivity fingerprint, which represents the overlap of each network within the pmfs component of each subject. (b) Polar plots showing the mean connectivity fingerprint of the three pmfs components (plotted outwards) with each of 17 resting-

state functional connectivity networks, across subjects. Resting-state networks with the highest overlap across subjects are labeled. (**c**) Left: Polar plots showing variability among 6 individual subjects. Right: Dissimilarity of the resting-state network fingerprints (variability in the connectivity fingerprint across subjects represented by the Wasserstein distance between unique subject pairs; **Methods**) are plotted as a function of each *pmfs* component for left and right hemispheres. Error bars represent 68% CI (SEM) across unique subject pairs.

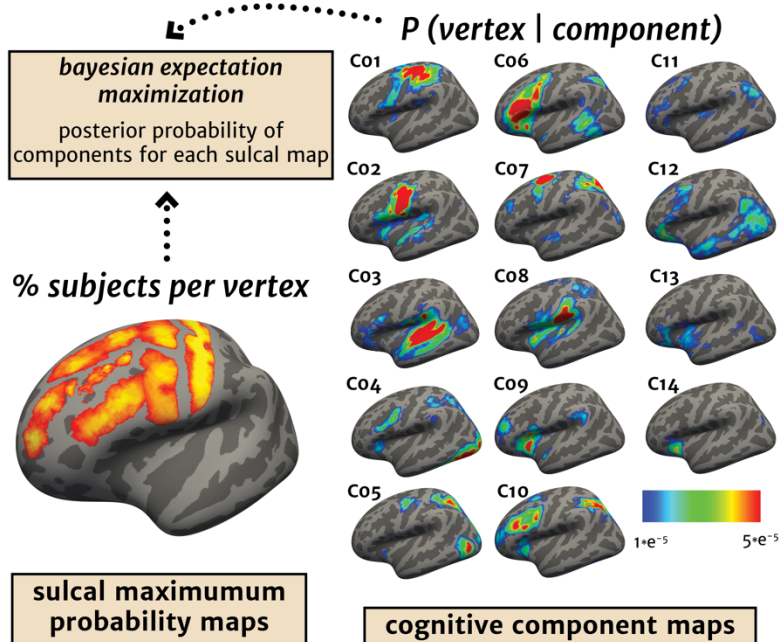
The pmfs-p, pmfs-i, and pmfs-a are functionally dissociable: Meta-analyses across 83 experimental task categories

We next tested if the functional dissociation of the *pmfs-p*, *pmfs-i*, and *pmfs-a* identified in individual subjects (**Fig. 4**) can also be observed in meta-analytic analyses of functional activation data at the group-level. To test for different patterns of functional activations across tasks, we generated sulcal probability maps on a template cortical surface (**Fig. 5a, bottom left**). Analogous to probabilistic maps for functional regions³⁷, the maps provide a vertex-wise measure of anatomical overlap across individuals for all 13 sulci in LPFC. As the *pmfs* components disappear on average templates (**Fig. 1**), these probabilistic maps are independent of the sulcal patterning of the template itself, which merely serves as a cortical surface independent of each individual cortical surface. We then compared these sulcal probability maps to 14 probabilistic “cognitive component” maps derived from an author-topic model of meta-analytic activation data across 83 experimental task categories. This model links patterns of brain activity to behavioral tasks via latent components representing putative functional subsystems.³⁸ Each cognitive component map (which was calculated on the same template cortical surface) provides the probability that a given voxel will be activated by each of the 14 components (across all 83 tasks). Using the cognitive component model, we then used expectation maximization to calculate the posterior probability (**Methods**) that each component would be engaged by brain activity with the same topography as each sulcal probability map (**Fig. 5a, right**). Importantly, when calculating the latter quantification, we implemented a leave-one-subject-out cross-validation procedure when constructing the sulcal probability maps in order to assess variability in the generated posterior

probabilities for each cognitive component (**Fig. 5b**). To indicate feasibility of this approach, the somato-motor components of the cognitive component map (C01, C02) align most highly with the central sulcus (**Supplemental Fig. 5**) as one would expect, which shows the ability of this method to measure structural-functional correspondences at the meta-analytic level.

This approach further reveals that the *pmfs-p*, *pmfs-i*, and *pmfs-a* are also functionally dissociable based on meta-analytic data of cognitive task activations. In the right hemisphere, the *pmfs-p*, *pmfs-i*, and *pmfs-a* showed distinct probabilities for separate cognitive components: 1) the *pmfs-p* loaded onto a default mode component (C11), 2) the *pmfs-i* loaded onto an executive function component (C10), and 3) the *pmfs-a* loaded onto an inhibitory control component (C09). In the left hemisphere, the *pmfs-a* and *pmfs-i* both loaded onto an executive function (C10) component, while the *pmfs-p* loaded onto an emotional processing/episodic memory component (C12). Like our individual subject analyses, there were also hemispheric differences: the cognitive components overlapping the most with the *pmfs-a* and *pmfs-p* differed between the two hemispheres. The *pmfs-p* loaded onto an emotional processing/episodic memory component in the left hemisphere (**Fig. 5b**, top row) and a default mode component in the right hemisphere (**Fig. 5b**, fourth row), while the *pmfs-a* loaded onto an executive function component in the left hemisphere (**Fig. 5b**, third row) and an inhibitory control component in the right hemisphere (**Fig. 5b**, bottom row).

a generating sulcal-functional mappings



b

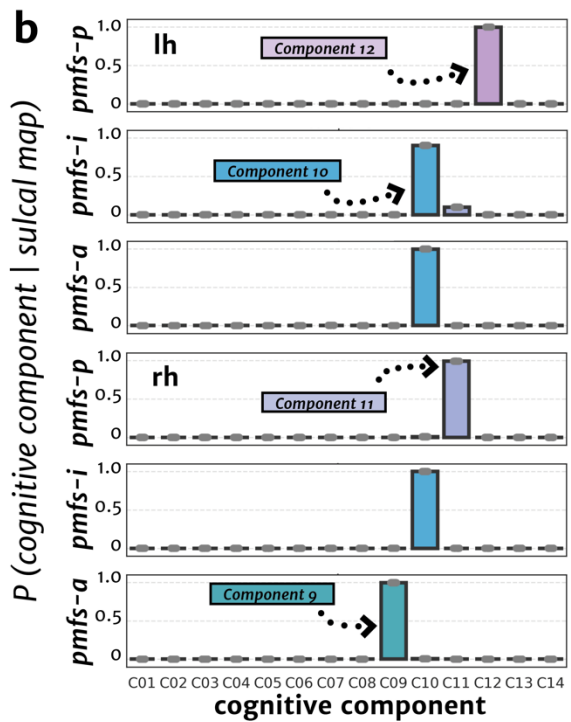


Figure 5. The pmfs-p, pmfs-i, and pmfs-a are functionally dissociable based on cognitive components: A meta-analysis of fMRI experimental tasks. (a) Schematic of analyses linking sulcal probability maps (bottom, left) and cognitive component maps (right) from a meta-analysis of fMRI experimental tasks³⁸ using an expectation maximization algorithm (**Methods**). For each pmfs component, the algorithm provides a posterior probability for each of 14 cognitive components being associated with the provided sulcal probability map. (b) For each pmfs component in each hemisphere, the posterior probability for each cognitive component is plotted. This approach reveals that the pmfs-p (Component 12, lh; Component 11, rh), pmfs-i (Component 10, lh and rh), and pmfs-a (Component 10, lh; Component 9, rh; **Methods**) are functionally dissociable based on meta-analytic data of cognitive task activations. Gray dots indicate individual subject data points when the analysis is performed with individual labels transformed to a template brain, rather than with probability maps.

Discussion

Here, we examined the relationship between cortical anatomy and function in human lateral prefrontal cortex (LPFC) with a two-pronged approach. First, we tested if a recent novel proposal of tertiary sulci in human LPFC in post-mortem brains²¹ could be applied to sulcal definitions of LPFC within *in-vivo* cortical surface reconstructions. Second, we tested if these tertiary LPFC sulcal definitions served as new landmarks for anatomical and functional gradients in LPFC. For the first time (to our knowledge), this two-pronged and multi-modal approach revealed that the posterior middle frontal sulcus (*pmfs*) is a sulcal landmark identifying transitions in anatomical and functional gradients within LPFC in individual subjects. Specifically, the *pmfs* is a characteristically shallow tertiary sulcus with three components that differ in their myelin content, resting state connectivity profiles, and engagement across meta-analyses of 83 cognitive tasks. We first discuss how these findings empirically support a classic, yet largely unconsidered, anatomical theory,^{12,39} as well as a recent cognitive neuroscience theory proposing a functional hierarchy in LPFC.^{5,40} We end by discussing a growing need for computational tools that automatically define tertiary sulci throughout cortex.

The anatomical-functional coupling in LPFC identified here is quite surprising considering the widespread literature providing little support for fine-grained anatomical-functional coupling in this cortical expanse and in association cortices more broadly when conducting traditional group-analyses^{41,42}. Indeed, cortical folding patterns relative to the location of anatomical, functional, or multimodal transitions are considered “imperfectly correlated”⁴³ in association cortices and especially in LPFC⁴⁴⁻⁴⁷. Contrary to these previous findings that did not consider tertiary sulci, the present findings support a classic, yet largely unconsidered theory proposed by Sanides (1962, 1964) that tertiary sulci serve as architectonic and functional landmarks in association cortices – and in particular, in LPFC^{12,39}. Specifically, Sanides proposed that because tertiary sulci emerge late in gestation and exhibit a protracted postnatal development, they likely serve as functional

Miller et al. | A new sulcal landmark in human prefrontal cortex

and architectonic landmarks in human association cortices, which also exhibit a protracted postnatal development. He further proposed that the late emergence and continued postnatal morphological development of tertiary sulci is likely related to protracted cognitive skills thought to be associated with LPFC such as sustained attention and executive functioning¹². Interestingly, identifying the three *pmfs* components quantified in the present study in his classic images shows myeloarchitectonic gradations among five areas in LPFC (**Fig. 6**).

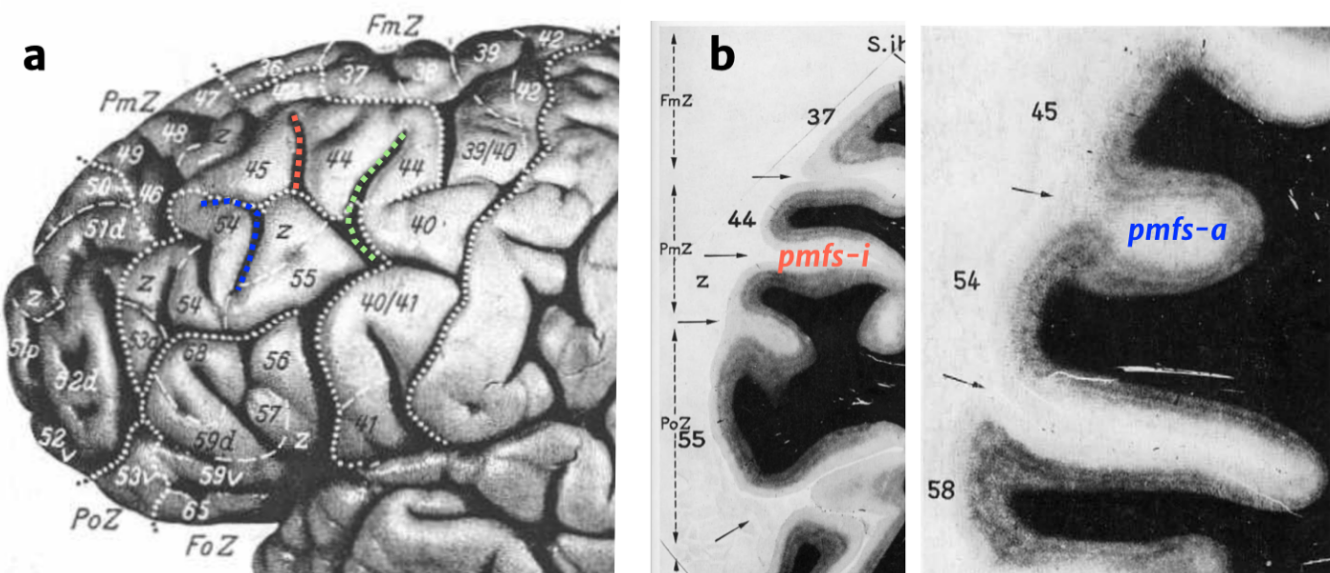


Figure 6. Linking the past to the present: Myelination gradients and the pmfs. (a) Photograph of a left hemisphere from Sanides (1962)³⁹. Numbers indicate cortical areas differing in myeloarchitecture. Dotted white lines: Sulcal boundaries as defined by Sanides. Dotted colored lines: *pmfs-p* (green), *pmfs-i* (red), and *pmfs-a* (blue) based on modern definitions²¹ used in the present study. Identifying *pmfs* components in Sanides' classic images shows that he identified myeloarchitectonic gradations within *pmfs* components, which is consistent with the present measurements. Gradations occurred in superior-inferior, as well as anterior-posterior dimensions. In the inferior portion of the *pmfs-p* (green), there is an anterior-posterior transition between areas 40 and 55. In the *pmfs-i* (red), there are two transitions: (i) a superior-inferior transition between areas 44 and a transition zone to area 55, and (ii) an anterior-posterior transition between areas 44 and 45. In the *pmfs-a*, there is a transition between areas 45 and 54. (b) Two myelination stains of histological sections (coronal orientation) from Sanides (1962)³⁹. Arrows indicate boundaries between labeled myeloarchitectonic areas (numbers). Components of the *pmfs* are labeled to help the reader link the myelination stains to the image at left.

In addition to supporting Sanides' classic anatomical theory^{12,39}, the present data demonstrated that the three *pmfs* components exhibit different resting-state connectivity profiles along a rostral-caudal axis, which builds on previous work also supporting a functional hierarchy along a rostral-caudal axis of LPFC. Further consistent with this hierarchy, evidence from neuroimaging, lesion, and electrocorticography studies indicate that this proposed rostral-caudal axis of LPFC is also related to levels of temporal and cognitive abstraction. That is, more anterior LPFC cortical regions are more highly engaged in tasks with higher abstract complexity^{5,6,40,48}. While there is axonal tracing data in non-human primates suggesting an anatomical basis for such a hierarchical organization⁴⁹⁻⁵¹, the present findings provide new evidence for a gradient of anatomically and functionally dissociable landmarks in LPFC that also support this hierarchical organization. Future work leveraging finer-scale multimodal and microanatomical data from individual human brains will be critical for uncovering anatomical and functional properties of LPFC across spatial and temporal scales that may further support the proposed functional rostral-caudal hierarchy of human LPFC.

Together, the culmination of present and previous findings show that tertiary sulci are landmarks in human VTC^{18,52-55}, medial PFC⁵⁶, and now, LPFC, as well as beg the question: How many other tertiary sulci serve as cortical landmarks? We stress that it is unlikely that all tertiary sulci will serve as cortical landmarks, since neuroanatomists have known for over a century that not all sulci function as cortical landmarks^{8,57-61}. Nonetheless, this does not preclude the importance of future studies identifying which tertiary sulci are architectonic, functional, behavioral, or multimodal landmarks – not only in healthy young adults as examined here, but also in developmental⁶² and clinical^{63,64} cohorts.

Such an exercise of carefully examining the relationship among tertiary sulci and multiple types of anatomical, functional, and behavioral data in individual subjects will require new neuroimaging tools to automatically identify tertiary sulci throughout human cortex. For instance,

Miller et al. | A new sulcal landmark in human prefrontal cortex

most neuroimaging software packages are only capable of automatically defining about 30-35 primary and secondary sulci in a given hemisphere⁶⁵. Current estimates approximate 107 sulci in each hemisphere when considering tertiary sulci²¹. Thus, studies in the immediate future will still require the manual identification of tertiary sulci, which is labor intensive and requires expertise¹. For example, the present study required manual definitions of over ~800 sulci in 72 hemispheres. While 72 is a large sample size compared to other labor-intensive anatomical studies in which 20 hemispheres is considered sufficient to encapsulate individual differences⁶⁶, 2400 hemispheres are available just from the HCP alone. Defining tertiary sulci in only the LPFC of every HCP participant would require ~26,400 manual definitions, while defining all tertiary sulci in the entire HCP dataset would require over a quarter of a million (~256,800) manual definitions. Consequently, manual identification of tertiary sulci will continue to limit sample sizes in immediate future studies until new automated methods are generated².

In the interim, we sought to leverage the anatomical labeling in this study to aid the field in the identification of sulcal landmarks in LPFC. The probability maps of sulcal locations in the present study are openly available and may be transformed to held-out individual brains (**Supplemental Fig. 7; Supplemental Results: Extensive individual differences in the location of the pmfs across individuals**). Accordingly, manual identification of these landmarks within individuals is greatly aided, allowing future studies to apply these tools to identify LPFC tertiary in individual subjects, including those from various groups such as patient or developmental cohorts.

¹ Classic neuroanatomy atlases provide schematics of sulci to guide the reader, as well as guide the practice of manual sulcal definitions. Modern atlases, including the recent proposal of tertiary sulci that we used to guide the manual definition of LPFC tertiary sulci (Petrides, 2019), continue this historical trend. Thus, defining tertiary sulci requires the expertise to apply a two-dimensional schematic of a post-mortem brain to an inflated cortical surface reconstruction. This application requires many translational steps including the fact that the schematic does not fully represent individual subject variability – an issue which has been brought up, but remains unresolved, for over a century. For example, in reference to his own images of sulci and cortical areas, Smith (1907) writes: "...no single example is the exact condition represented in these schemata..." (Smith, 1907, pg. 238).

² To our knowledge, and to quote Klein and colleagues, the "Mindboggle-101 dataset is still the largest publicly available set of manually edited human brain labels in the world" (Klein et al., 2017). Consisting of 101 brains (202 hemispheres), the dataset contains only 31 labels in each hemisphere.

Miller *et al.* | A new sulcal landmark in human prefrontal cortex

Because smaller tertiary sulci in association cortex are the latest sulcal indentations to develop^{12,57}, their anatomical trajectories and properties likely relate to the development of cognitive abilities associated with the LPFC and other association areas as Sanides hypothesized, which recent ongoing work supports⁶². Moving forward, we hope to leverage the manual labeling performed here to develop better automated algorithms for sulcal labeling within individuals. Future work using deep learning algorithms and expanded training data may help to identify tertiary structures in novel brains without manual labeling or intervention⁶⁷. Such automated tools have translational applications as tertiary sulci are largely hominoid-specific structures²⁶ located in association cortices associated with many neurological disorders. Thus, morphological features of these under-studied neuroanatomical structures may be biomarkers useful for future diagnostic purposes. To begin to achieve this goal and to aid the field, we are making our probabilistic maps of tertiary sulci in LPFC freely available with the publication of this paper.

Methods

In the sections below, we describe the data used and the analysis methods implemented in three separate sections: 1) the general approach and a description of the multi-modal datasets that were used, 2) a detailed description of the methodology used for sulcal labeling within individual subjects, and 3) the calculation of anatomical and functional metrics.

General approach

We sought to characterize sulcal morphology at the individual subject level in the lateral prefrontal cortex (LPFC) of the human brain. To implement this process, we manually defined sulci following the most recent and comprehensive proposed labeling of sulci in the frontal lobe based on post-mortem specimens^{21,22}. As in our prior work⁵³, all sulci were defined in native space cortical surfaces and individual hemispheres, which enables the most accurate definition of tertiary sulci in *in-vivo* neuroimaging data.

Multi-modal HCP dataset

We analyzed a subset of the multi-modal imaging data available for individual subjects from the Human Connectome Project (HCP). We began with the first 5 numerically listed HCP subjects and then randomly selected 31 additional human subjects from the HCP for a total of 36 individuals (17 female, 19 male, age range 22-36 years).

Anatomical T₁-weighted (T_{1-w}) MRI scans (0.8 mm voxel resolution) were obtained in native space from the HCP database, along with outputs from the HCP modified FreeSurfer pipeline (see Glasser et al., 2013 for T1 and FreeSurfer pipeline details)⁶⁸. Maps of the ratio of T₁-weighted and T₂-weighted scans, which is a measure of tissue contrast enhancement related to myelin content, were downloaded as part of the HCP ‘Structural Extended’ release. All additional

Miller et al. | A new sulcal landmark in human prefrontal cortex

anatomical metrics, which are detailed in the next section, were calculated on the full-resolution, native FreeSurfer (<https://surfer.nmr.mgh.harvard.edu/>) meshes⁶⁹.

Anatomical labeling and metrics

Manual sulcal labeling

Guided by a recent comprehensive proposal for labeling sulci in LPFC^{21,22}, each sulcus was manually defined within each individual hemisphere on the FreeSurfer *inflated* mesh with *tksurfer*. The *curvature* metric in FreeSurfer distinguished the boundaries between sulcal and gyral components, and manual lines were drawn to separate sulcal components based upon the proposal by Petrides and colleagues (2012; 2019), as well as the appearance of sulci across the *inflated*, *pial*, and *smoothwm* surfaces. We maintained the number of components for all sulci (e.g., the three components of the *posterior middle frontal sulcus* - *pmfs*) based on the proposal by Petrides and colleagues to test if each of these sulcal components could be defined in a relatively large sample size (N=72) of individual, *in-vivo* hemispheres. That is, the proposal for defining sulci in LPFC that is included in the book chapter²² and most recent atlas²¹ are summarized as a schematic. It is unclear from which data (or series of data) this schematic was generated as - to our knowledge - there have been no empirical papers published with these sulcal definitions and morphological analyses in individual hemispheres until the present work. Consequently, our definitions were identical to the proposal in order to test whether this distinction among sulci that is summarized in the schematic could be applied to empirical data in individual hemispheres. The labels were generated using a two-tiered procedure. The labels were first defined manually by J.M. and J.Y. and then finalized by a neuroanatomist (K.S.W.). All anatomical labels for a given hemisphere were fully defined before any morphological or functional analysis of the sulcal labels was performed. The superior, inferior, posterior, and anterior boundaries of our cortical expanse of interest were the following sulci, respectively: (1) the anterior and posterior components of the *superior frontal sulcus*, (2) the *inferior frontal sulcus*, (3) the *central sulcus*,

Miller et al. | A new sulcal landmark in human prefrontal cortex

and (4) the horizontal (*imfs-h*) and vertical (*imfs-v*) intermediate frontal sulci. An example hemisphere with every sulcus labeled within these boundaries is shown in **Fig. 2**, and the *pmfs* sulcal components are plotted on each hemisphere in **Supplemental Fig. 1**.

Quantification of sulcal depth and surface area

Sulcal depth was calculated from the native meshes generated by the FreeSurfer HCP pipeline. Raw mm values for sulcal depth were calculated from the sulcal fundus to the smoothed outer pial surface using a custom-modified version of a recently developed algorithm for robust morphological statistics building on the FreeSurfer pipeline²⁹. Surface area (mm²) was generated for each sulcus through the *mris_anatomical_stats* function in FreeSurfer. We focused on sulcal depth as it is the main measurement that is used to discriminate tertiary sulci from primary and secondary sulci. Specifically, primary sulci are deepest, while tertiary sulci are shallowest, and secondary sulci are in between⁵⁷. We also included surface area as tertiary sulci typically also have a reduced surface area compared to primary and secondary sulci.

Cross-validation of sulcal location

In order to quantify the ability to predict the location of each sulcus across subjects, we registered all sulcal labels to a common template surface (*fsaverage*) using cortex-based alignment⁶⁹. Similarity between each transformed individual label and the labels defined on *fsaverage* was calculated via the DICE coefficient, where X and Y are each label:

$$DICE(X, Y) = \frac{2|X \cap Y|}{|X| + |Y|}$$

The cortex-based alignment algorithm uses 6 primary sulcal landmarks to register subjects including the central sulcus, meaning that the DICE coefficients for the *central sulcus* are biased towards being high and with minimal variability. However, because this does not affect the other

Miller et al. | A new sulcal landmark in human prefrontal cortex

lateral frontal sulci, the central sulcus is included as a proxy noise ceiling measurement for DICE coefficient values.

Sulcal probability maps were calculated to describe the vertices with the highest alignment across subjects for a given sulcus. A map was generated for each sulcus by calculating, at each vertex in the *fsaverage* hemisphere, the number of subjects with that vertex labeled as the given sulcus, divided by the total number of subjects. In order to avoid overlap among sulci, we then constrained the probability maps into *maximum probability maps* (MPMs) by only including vertices where (1) greater than 33% of subjects included the given sulcal label and (2) the sulcus with the highest value of subject overlap was assigned to a given vertex. In a leave-one-subject out cross-validation procedure, we generated probability maps from $n = 35$ subjects and registered the probability map to the held-out subject's native cortical surface. This provided a measure of sulcal variability and prediction accuracy (**Supplemental Fig. 6**). This procedure also allows the identification of the *pmfs* sulcal components within held-out individual subjects, reducing the extent of manual labeling necessary to identify this structure. Finally, the MPMs were used when analyzing meta-analytical functional data (described in the section *Cognitive Component Modeling*). The MPMs and code for alignment to new subjects will be available on OSF with the publication of this paper.

Calculating T_{1w}/T_{2w} myelin index along an anterior-posterior gradient in LPFC

In order to test if there is a relationship between any of our sulci of interest and myelination content, we used an *in vivo* proxy of myelination: the T_{1w}/T_{2w} maps for each individual hemisphere.^{31,43} We averaged this value across each vertex for each sulcus in order to demonstrate if the *pmfs* sulcal components are separable based on myelin content (**Fig. 3**). We further sought to characterize the relationship between morphology and myelin by determining if there was an anterior-posterior gradient of myelination across individual hemispheres. First, for each individual hemisphere, we calculated the minimum geodesic distance of each vertex from

Miller et al. | A new sulcal landmark in human prefrontal cortex

the central sulcus. Geodesic distance was calculated on the *fiducial* surface using algorithms in the pycortex (<https://gallantlab.github.io/>) package.⁷⁰ Then, we averaged across the vertices within each sulcus and tested for a linear relationship between average distance from the central sulcus and myelin content. To take advantage of each subject's individual data, we built a mixed linear model (random intercepts) in the lme4 R package, using sulci and hemisphere as explanatory variables to predict average myelin content (**Fig. 3**).

Functional metrics

Resting-state network topology

In order to calculate if the three *pmfs* sulcal components were functionally distinct from one another, we calculated functional connectivity network profiles for each sulcus. Resting-state network parcellations for each individual subject were used from Kong et al. (2018), who generated individual network definitions by applying a hierarchical Bayesian network algorithm to produce maps for each of 17-networks⁷¹ in individual HCP subjects. These data were calculated in the template HCP *fs_LR 32k* space. We resampled the network profiles for each subject onto the *fsaverage* cortical surface and, then, to each native surface using CBIG tools (<https://github.com/ThomasYeoLab/CBIG>). We then calculated the overlap of each *pmfs* sulcus in each subject with each of the 17 resting-state networks. We also separated the components of the *pmfs* and tested whether they showed similar or different network connectivity profiles using a 3-way repeated-measures ANOVA (sulcal component x network x hemisphere). Variability across individuals in the network profiles for each *pmfs* component was calculated by generating the Wasserstein metric (Earth Mover's Distance) between the resting-state network overlap values for each unique subject pair (**Fig. 4b**).

Cognitive component modeling

To further examine if the functional dissociation of the *pmfs-p*, *pmfs-i*, and *pmfs-a* is also identifiable using meta-analytic functional MRI (fMRI) data, we quantified the overlap between the *maximum probability maps* (MPMs) of each sulcal component and meta-analytic fMRI data from hundreds of experiments aligned to the *fsaverage* surface. Specifically, we quantitatively related the sulcal MPMs to vertex-wise maps for 14 cognitive components, detailing how each vertex relates to a given set of cognitive operations across tasks and experiments³⁸. We used a Bayesian method of expectation maximization to determine the combination of cognitive components that best fit each sulcal MPM. This resulted in a set of probabilities for each cognitive component for each sulcal map. We tested whether all sulci and the three components of the *pmfs* were distinguishable based upon these cognitive component loadings from a repeated-measures ANOVA (**Fig. 5**).

Statistical methods

All repeated measures ANOVAs (including sphericity correction) and post-hoc testing were performed with the *afex* and *emmeans* R packages, imported into Python via *rpy2*. For each ANOVA, cortical hemisphere and sulcus were used as within-subject factors. Effect sizes for each main effect and interaction were calculated and reported with the *generalized eta-squared* metric. Mixed linear models were implemented in the *lme4* R package.

Cortical surface files were loaded in and operated on in Python using the *nilearn* software:

<https://nilearn.github.io>

Data availability

The raw data in the present work is publicly available from the Human Connectome Project (HCP):

[https://www.humanconnectome.org/study/hcp-young-adult/document/1200-subjects-data-](https://www.humanconnectome.org/study/hcp-young-adult/document/1200-subjects-data-release/)

[release\)](#)/ The HCP dataset and processing are described in previous publications^{43,68}. The probability maps for LPFC sulcal definitions along with anatomical statistics for each manually labeled sulcus and analysis code will be freely available with the publication of the paper.

Author Contributions

Manual anatomical labeling: J.A.M., W.V., K.S.W. Data analysis and interpretation of the data: J.A.M., D.J.L., K.S.W. Drafting paper: J.A.M, K.S.W. Revising paper: J.A.M, W.V., D.J.L., M.D., K.S.W. Supervision and study conceptualization: J.A.M., M.D, K.S.W.

Acknowledgments

This work was supported by (1) start-up funds provided by the University of California, Berkeley and the Helen Wills Neuroscience Institute (K.S.W.); (2) NIH grant RO1 MH63901 (J.A.M., M.D.). We also thank Jewelia Yao for help with the manual definition of LPFC sulci.

References

- 1 Mesulam, M. From sensation to cognition. *Brain* **121**, 1013-1052 (1998).
- 2 Miller, E. K. & Cohen, J. D. AN INTEGRATIVE THEORY OF PREFRONTAL CORTEX FUNCTION. *Annu Rev Neurosci* **24**, 167-202 (2001).
- 3 Donahue, C. J., Glasser, M. F., Preuss, T. M., Rilling, J. K. & Van Essen, D. C. Quantitative assessment of prefrontal cortex in humans relative to nonhuman primates. *Proc Natl Acad Sci U S A*, doi:10.1073/pnas.1721653115 (2018).
- 4 Szczepanski, S. M. & Knight, R. T. Insights into human behavior from lesions to the prefrontal cortex. *Neuron* **83**, 1002-1018, doi:10.1016/j.neuron.2014.08.011 (2014).
- 5 Badre, D. & D'Esposito, M. Is the rostro-caudal axis of the frontal lobe hierarchical? *Nat Rev Neurosci* **10**, 659-669, doi:10.1038/nrn2667 (2009).
- 6 Voytek, B. et al. Oscillatory dynamics coordinating human frontal networks in support of goal maintenance. *Nat Neurosci* **18**, 1318-1324, doi:10.1038/nn.4071 (2015).
- 7 Nee, D. E. & D'Esposito, M. The hierarchical organization of the lateral prefrontal cortex. *eLife* **5**, doi:10.7554/eLife.12112 (2016).
- 8 Zilles, K., Palomero-Gallagher, N. & Amunts, K. Development of cortical folding during evolution and ontogeny. *Trends Neurosci* **36**, 275-284, doi:10.1016/j.tins.2013.01.006 (2013).
- 9 Van Essen, D. C. & Dierker, D. L. Surface-based and probabilistic atlases of primate cerebral cortex. *Neuron* **56**, 209-225, doi:10.1016/j.neuron.2007.10.015 (2007).
- 10 Van Essen, D. & Drury, H. A. Structural and Functional Analyses of Human Cerebral Cortex Using a Surface-Based Atlas. *The Journal of Neuroscience* **17**, 7079-7102 (1997).
- 11 Zilles, K., Armstrong, E., Schleicher, A. & Krestschmann, H. J. The human pattern of gyration in the cerebral cortex. *Anat Embryol* **179** (1988).
- 12 Sanides, F. STRUCTURE AND FUNCTION OF THE HUMAN FRONTAL LOBE. *Neuropsychologia* **2**, 209-219 (1964).
- 13 Gazzaley, A. & Nobre, A. C. Top-down modulation: bridging selective attention and working memory. *Trends Cogn Sci* **16**, 129-135, doi:10.1016/j.tics.2011.11.014 (2012).
- 14 Feredoes, E., Heinen, K., Weiskopf, N., Ruff, C. & Driver, J. Causal evidence for frontal involvement in memory target maintenance by posterior brain areas during distracter interference of visual working memory. *Proc Natl Acad Sci U S A* **108**, 17510-17515, doi:10.1073/pnas.1106439108 (2011).
- 15 Jung, R. E. & Haier, R. J. The Parieto-Frontal Integration Theory (P-FIT) of intelligence: Converging neuroimaging evidence. *Behav Brain Sci* **30**, 135+, doi:10.1017/S0140525x07001185 (2007).
- 16 Curtis, C. E. & D'Esposito, M. Persistent activity in the prefrontal cortex during working memory. *Trends Cogn Sci* **7**, 415-423 (2003).
- 17 Garcia-Cabezas, M. A., Zikopoulos, B. & Barbas, H. The Structural Model: a theory linking connections, plasticity, pathology, development and evolution of the cerebral cortex. *Brain Struct Funct*, doi:10.1007/s00429-019-01841-9 (2019).
- 18 Weiner, K. S., Natu, V. S. & Grill-Spector, K. On object selectivity and the anatomy of the human fusiform gyrus. *Neuroimage* **173**, 604-609, doi:10.1016/j.neuroimage.2018.02.040 (2018).
- 19 Gordon, E. M. et al. Precision Functional Mapping of Individual Human Brains. *Neuron*, doi:10.1016/j.neuron.2017.07.011 (2017).
- 20 Kong, R. et al. Spatial Topography of Individual-Specific Cortical Networks Predicts Human Cognition, Personality, and Emotion. *Cereb Cortex*, doi:10.1093/cercor/bhy123 (2018).

- 21 Petrides, M. *Atlas of the Morphology of the Human Cerebral Cortex on the Average MNI Brain*. 1 edn, (Elsevier, 2019).
- 22 Petrides, M. & Pandya, D. N. in *The Human Nervous System* (eds J. Mai & G. Paxinos) Ch. 26, 988-1011 (Elsevier, 2012).
- 23 Connolly, C. *External Morphology of the Primate Brain*. (1950).
- 24 Eberstaller, O. *Das Stirnhirn*. (Urban & Schwarzenberg, 1890).
- 25 Rajkowska, G. & Goldman-Rakic, P. S. Cytoarchitectonic Definition of Prefrontal areas in the Normal Human Cortex: II. Variability in Locations of Areas 9 and 46 and Relationship to the Talairach Coordinate System. *Cereb Cortex* **5** (1995).
- 26 Amiez, C. et al. Sulcal organization in the medial frontal cortex provides insights into primate brain evolution. *Nat Commun* **10**, 3437, doi:10.1038/s41467-019-11347-x (2019).
- 27 Retzius, G. *Das Menschenhirn*. (Norstedt and Soener, 1896).
- 28 Ding, S. L. et al. Comprehensive cellular-resolution atlas of the adult human brain. *J Comp Neurol* **524**, 3127-3481, doi:10.1002/cne.24080 (2016).
- 29 Madan, C. R. Robust estimation of sulcal morphology. *Brain Inform* **6**, 5, doi:10.1186/s40708-019-0098-1 (2019).
- 30 Shams, Z., Norris, D. G. & Marques, J. P. A comparison of in vivo MRI based cortical myelin mapping using T1w/T2w and R1 mapping at 3T. *PLoS One* **14**, e0218089, doi:10.1371/journal.pone.0218089 (2019).
- 31 Glasser, M. F. & Van Essen, D. C. Mapping human cortical areas in vivo based on myelin content as revealed by T1- and T2-weighted MRI. *J Neurosci* **31**, 11597-11616, doi:10.1523/JNEUROSCI.2180-11.2011 (2011).
- 32 Vogt, C. & Vogt, O. Allgemeinere ergebnisse unserer hirnforschung. *J. Psychol. Neurol.* **25**, 279-462 (1919).
- 33 Hopf, A. Über die Verteilung myeloarchitektonischer Merkmale in der Stirnhirnrinde beim Menschen. *J. Hirnforsch* **2**, 311-333 (1956).
- 34 Flechsig, P. *Anatomie des Menschlichen Gehirns und Rückenmarks auf Myelogenetischer Grundlage*. (1920).
- 35 Dick, F. et al. In vivo functional and myeloarchitectonic mapping of human primary auditory areas. *J Neurosci* **32**, 16095-16105, doi:10.1523/JNEUROSCI.1712-12.2012 (2012).
- 36 Seitzman, B. A. et al. Trait-like variants in human functional brain networks. *Proc Natl Acad Sci U S A* **116**, 22851-22861, doi:10.1073/pnas.1902932116 (2019).
- 37 Wang, L., Mruczek, R. E., Arcaro, M. J. & Kastner, S. Probabilistic Maps of Visual Topography in Human Cortex. *Cereb Cortex* **25**, 3911-3931, doi:10.1093/cercor/bhu277 (2015).
- 38 Yeo, B. T. et al. Functional Specialization and Flexibility in Human Association Cortex. *Cereb Cortex* **25**, 3654-3672, doi:10.1093/cercor/bhu217 (2015).
- 39 Sanides, F. in *Monographien aus dem Gesamtgebiete der Neurologie und Psychiatrie* Vol. 98 (eds M. Muller, H. Spatz, & P. Vogel) 176-190 (Springer Berlin Heidelberg, 1962).
- 40 Badre, D. & Nee, D. E. Frontal Cortex and the Hierarchical Control of Behavior. *Trends Cogn Sci* **22**, 170-188, doi:10.1016/j.tics.2017.11.005 (2018).
- 41 Vazquez-Rodriguez, B. et al. Gradients of structure-function tethering across neocortex. *Proc Natl Acad Sci U S A* **116**, 21219-21227, doi:10.1073/pnas.1903403116 (2019).
- 42 Paquola, C. et al. Microstructural and functional gradients are increasingly dissociated in transmodal cortices. *PLoS Biol* **17**, e3000284, doi:10.1371/journal.pbio.3000284 (2019).
- 43 Glasser, M. F. et al. A multi-modal parcellation of human cerebral cortex. *Nature* **536**, 171-178, doi:10.1038/nature18933 (2016).
- 44 Van Essen, D. C., Glasser, M. F., Dierker, D. L. & Harwell, J. Cortical parcellations of the macaque monkey analyzed on surface-based atlases. *Cereb Cortex* **22**, 2227-2240, doi:10.1093/cercor/bhr290 (2012).

- 45 Caspers, S., Eickhoff, S. B., Zilles, K. & Amunts, K. Microstructural grey matter parcellation and its relevance for connectome analyses. *Neuroimage* **80**, 18-26, doi:10.1016/j.neuroimage.2013.04.003 (2013).
- 46 Robinson, E. C. et al. MSM: a new flexible framework for Multimodal Surface Matching. *Neuroimage* **100**, 414-426, doi:10.1016/j.neuroimage.2014.05.069 (2014).
- 47 Coalson, T. S., Van Essen, D. C. & Glasser, M. F. The impact of traditional neuroimaging methods on the spatial localization of cortical areas. *Proc Natl Acad Sci U S A* **115**, E6356-E6365, doi:10.1073/pnas.1801582115 (2018).
- 48 Koechlin, E., Ody, C. & Kouneiher, F. The Architecture of Cognitive Control in the Human Prefrontal Cortex. *Science* **302** (2003).
- 49 Thiebaut de Schotten, M., Dell'Acqua, F., Valabregue, R. & Catani, M. Monkey to human comparative anatomy of the frontal lobe association tracts. *Cortex* **48**, 82-96, doi:10.1016/j.cortex.2011.10.001 (2012).
- 50 Goulas, A., Majka, P., Rosa, M. G. P. & Hilgetag, C. C. A blueprint of mammalian cortical connectomes. *PLoS Biol* **17**, e2005346, doi:10.1371/journal.pbio.2005346 (2019).
- 51 Goulas, A., Uylings, H. B. & Stiers, P. Mapping the hierarchical layout of the structural network of the macaque prefrontal cortex. *Cereb Cortex* **24**, 1178-1194, doi:10.1093/cercor/bhs399 (2014).
- 52 Lorenz, S. et al. Two New Cytoarchitectonic Areas on the Human Mid-Fusiform Gyrus. *Cereb Cortex* **27**, 373-385, doi:10.1093/cercor/bhv225 (2017).
- 53 Weiner, K. S. et al. The mid-fusiform sulcus: a landmark identifying both cytoarchitectonic and functional divisions of human ventral temporal cortex. *Neuroimage* **84**, 453-465, doi:10.1016/j.neuroimage.2013.08.068 (2014).
- 54 Caspers, J. et al. Cytoarchitectonical analysis and probabilistic mapping of two extrastriate areas of the human posterior fusiform gyrus. *Brain Struct Funct* **218**, 511-526, doi:10.1007/s00429-012-0411-8 (2013).
- 55 Nasr, S. et al. Scene-selective cortical regions in human and nonhuman primates. *J Neurosci* **31**, 13771-13785, doi:10.1523/JNEUROSCI.2792-11.2011 (2011).
- 56 Lopez-Persem, A., Verhagen, L., Amiez, C., Petrides, M. & Sallet, J. The Human Ventromedial Prefrontal Cortex: Sulcal Morphology and Its Influence on Functional Organization. *J Neurosci* **39**, 3627-3639, doi:10.1523/JNEUROSCI.2060-18.2019 (2019).
- 57 Welker, W. (eds A. Peters & E.G. Jones) 3-136 (Plenum Press, 1990).
- 58 Ono, M., Kubik, S. & Abernathey, C. *Atlas of the Cerebral Sulci* (Thieme Medical Publishers, Inc. , 1990).
- 59 Smith, G. E. A New Topographical Survey of the Human Cerebral Cortex, being an Account of the Distribution of the Anatomically Distinct Cortical Areas and their Relationship to the Cerebral Sulci. *J Anat Physiol* **41**, 237-254 (1907).
- 60 Van Essen, D. C. et al. Cerebral cortical folding, parcellation, and connectivity in humans, nonhuman primates, and mice. *Proc Natl Acad Sci U S A*, doi:10.1073/pnas.1902299116 (2019).
- 61 Bailey, P. & Bonin, G. V. *The Isocortex of Man*. Vol. 1 (University of Illinois Press, 1951).
- 62 Voorhies, W. et al. in *Experimental Biology* (San Diego, CA, 2020).
- 63 Parker, B. J. The role of sulcal morphology in developmental prosopagnosia. *Open Science Framework* (2019).
- 64 Brun, L. et al. Localized Misfolding Within Broca's Area as a Distinctive Feature of Autistic Disorder. *Biol Psychiatry Cogn Neurosci Neuroimaging* **1**, 160-168, doi:10.1016/j.bpsc.2015.11.003 (2016).
- 65 Destrieux, C., Fischl, B., Dale, A. & Halgren, E. Automatic parcellation of human cortical gyri and sulci using standard anatomical nomenclature. *Neuroimage* **53**, 1-15, doi:10.1016/j.neuroimage.2010.06.010 (2010).

- 66 Amunts, K. & Zilles, K. Architectonic Mapping of the Human Brain beyond Brodmann. *Neuron* **88**, 1086-1107, doi:10.1016/j.neuron.2015.12.001 (2015).
- 67 Hao, L. et al. in *IEEE International Symposium on Biomedical Imaging (ISBI)* (Iowa City, IA, 2020).
- 68 Glasser, M. F. et al. The minimal preprocessing pipelines for the Human Connectome Project. *Neuroimage* **80**, 105-124, doi:10.1016/j.neuroimage.2013.04.127 (2013).
- 69 Fischl, B., Sereno, M. I., Tootell, R. B. H. & Dale, A. M. High-Resolution Intersubject Averaging and a Coordinate System for the Cortical Surface. *Human Brain Mapping* **8**, 272-284 (1999).
- 70 Gao, J. S., Huth, A. G., Lescroart, M. D. & Gallant, J. L. Pycortex: an interactive surface visualizer for fMRI. *Front Neuroinform* **9**, 23, doi:10.3389/fninf.2015.00023 (2015).
- 71 Yeo, B. T. et al. The organization of the human cerebral cortex estimated by intrinsic functional connectivity. *J Neurophysiol* **106**, 1125-1165, doi:10.1152/jn.00338.2011 (2011).